RESEARCH ARTICLE | JULY 05 2023

Improved energy storage performance in rare-earth modified lead-free BNT-based relaxor ferroelectric ceramics

Chengwen Bin ; Xu Hou ; Luocheng Liao; Yuwen Liu; Han Yang ; Yunya Liu ; Jie Wang

Appl. Phys. Lett. 123, 012901 (2023)
https://doi.org/10.1063/5.0158219

Applied Physics Letters ARTICLE pubs.aip.org/aip/apl

Improved energy storage performance in rare-earth modified lead-free BNT-based relaxor ferroelectric ceramics

Cite as: Appl. Phys. Lett. **123**, 012901 (2023); doi: 10.1063/5.0158219
Submitted: 15 May 2023 · Accepted: 14 June 2023 ·
Published Online: 5 July 2023

View Online Export Citation CrossMark

Chengwen Bin,[1] Xu Hou,[1,2] Luocheng Liao,[3] Yuwen Liu,[1] Han Yang,[1,4] Yunya Liu,[3] and Jie Wang[1,5,6,a)]

AFFILIATIONS

[1]Department of Engineering Mechanics, Zhejiang University, Hangzhou, Zhejiang 310027, China
[2]Department of Industrial and Systems Engineering, The Hong Kong Polytechnic University, Hung Hom, Kowloon, Hong Kong, China
[3]Key Laboratory of Low Dimensional Materials and Application Technology of Ministry of Education, School of Materials Science and Engineering, Xiangtan University, Xiangtan 411105, Hunan, China
[4]Key Laboratory of Electromagnetic Wave Information Technology and Metrology of Zhejiang Province, College of Information Engineering, China Jiliang University, Hangzhou 310018, China
[5]Zhejiang Laboratory, Hangzhou, Zhejiang 311100, China
[6]Key Laboratory of Soft Machines and Smart Devices of Zhejiang Province, Zhejiang University, Hangzhou, Zhejiang 310027, China

[a)]**Author to whom correspondence should be addressed:** jw@zju.edu.cn

ABSTRACT

Dielectric ceramic capacitors with high energy storage performance are indispensable components in high-power pulse electronic systems. Herein, a collaborative optimization design is employed to achieve excellent energy storage performance in rare-earth oxides modified $0.76(0.94Bi_{0.5}Na_{0.5}TiO_3\text{-}0.06BaTiO_3)\text{-}0.24Sr_{0.7}Bi_{0.2}TiO_3$ (BNBT-SBT) ceramics by simultaneously enhancing the breakdown field strength (E_b) and relaxor behavior. To this end, ferroelectric domains are partially transformed into polar nanoregions by introducing relaxor ferroelectric SBT, while a smaller grain size is produced by doping rare-earth elements to improve the E_b and further disrupt the long-range order of ferroelectric polarization. It is found that the La-doped BNBT-SBT ceramic simultaneously exhibits a superior energy storage density of 4.4 J cm^{-3} and an ultrahigh efficiency of ~91% under a moderate electric field of 300 kV/cm. The good temperature stability (30–120 °C), frequency endurance (1–100 Hz), electric fatigue resistance (1–10^6 cycles), and excellent power density (108 MW cm^{-3}) are also obtained in the lead-free $Bi_{0.5}Na_{0.5}TiO_3$-based relaxor ferroelectric ceramics. These prominent properties indicate that the La-doped BNBT-SBT ceramic is a promising candidate for applications of high-energy storage capacitors.

With the increase in global energy consumption and the emergence of numerous environmental issues, it is urgent to develop efficient and clean energy storage devices.[1,2] Among the devices developed for this purpose, dielectric capacitors have unique potential in pulse power applications, which require significant power density, moderate energy storage density, and millisecond level ultra-fine charge and discharge rates. The main parameters of dielectric capacitors include energy storage density (W_{rec}) and efficiency (η), which can be calculated by $W_{tol} = \int_0^{Pm} EdP$, $W_{rec} = \int_{Pr}^{Pm} EdP$, and $\eta = \frac{W_{rec}}{W_{tol}} \times 100\%$, where P_m and P_r are the maximum and remanent polarizations, respectively,[3] and E is the applied electric field. According to the calculation formula, a large $\Delta P(P_m\text{-}P_r)$ and high breakdown field strength (E_b) are essential to enhance the W_{rec} and η simultaneously.

Recently, ceramic capacitors have been widely investigated for energy storage due to their prominent thermal stability, stable mechanical properties, and high dielectric permittivity.[4,5] Relaxor ferroelectric ceramics usually possess high P_m, low P_r, and moderate E_b compared with normal ferroelectric materials, which is beneficial for achieving excellent energy storage performance.[6] Lead-free $Bi_{0.5}Na_{0.5}TiO_3$ (BNT) ceramic is an important system of relaxor ferroelectrics, which exhibits outstanding ferroelectric property and high Curie temperature (320 °C).[7] However, its remanent polarization and

coercive field are large while the breakdown field strength is low, which prevent its application in energy storage devices. Several engineering modulations have been used to improve the energy storage performance of BNT-based ceramics.[6] For example, Zhang *et al.* reported a novel $LiTaO_3$ (LT) modified 0.93BNT-0.07LT ceramic ($W_{rec} \sim 3.1$ J cm^{-3}, $\eta \sim 74.2\%$),[8] in which LT could improve the relaxor behavior and suppress the early polarization saturation. Hu *et al.* obtained a good W_{rec} of 2.41 J cm^{-3} in the $Bi_{0.5}Na_{0.5}TiO_3$–$(Na_{0.73}Bi_{0.09})NbO_3$ (BNT-NBN) system via domain engineering,[9] in which the introduction of NBN could reduce grain size and oxygen vacancy concentration, which is benefit for the improvement of E_b.

In general, abnormal and excellent ferroelectric properties are expected to be obtained near the morphotropic phase boundary (MPB).[7] $BaTiO_3$ (BT) can be introduced into the BNT system to create a solid solution and related MPB.[10–12] The 0.94BNT-0.06BT ceramics at MPB possess a coexisting of rhombohedral (R) and tetragonal (T) phases over a wide temperature range,[12] which results in strong ferroelectric properties such as larger polarization and enhanced domain wall switching ability. Hence, the 0.94BNT-0.06BT system is herein chosen as the base composition to develop new materials with excellent energy storage performance. Obviously, the strong ferroelectric hysteresis, large P_r and insufficient E_b of the pure 0.94BNT-0.06BT system needs to be modified by destroying the long-term ferroelectric order, enhancing the polar nanoregions (PNRs) and strengthening the E_b. $(Sr_{0.7}Bi_{0.2})TiO_3$ (SBT) is a type of relaxor ferroelectric, which shows broadened dielectric maxima with a perovskite structure.[13] (The charge imbalance is caused by Bi^{3+} replacing Sr^{2+}.) Therefore, SBT was used to form a solid solution with BNT-BT, which could break the long-range order and achieve better relaxor behavior.[14] Due to the valence imbalance and high temperature activation, a lot of oxygen vacancies or pores exist in SBT, leading to leakage conductivity loss and low E_b.[15] This disadvantage is also revealed in the BNT-BT-SBT composite ceramics. Therefore, further optimization scheme is necessary.

Rare-earth elements are common dopants to improve the ferroelectric properties of perovskite materials, which will decrease the dielectric loss and grain size, then further enhance the E_b.[16–19] Consequently, the rare-earth elements doping is expected to be an effective mean for improving the energy storage performance of BNT-based ceramics. In this work, a two-step optimization strategy is designed to obtain superior energy storage performance in BNT-based ceramics, as displayed in Fig. S1. First, SBT was introduced to partially transform the ferroelectric domains into polar nanoregions (PNRs). Then, three rare-earth elements (La, Er, and Nd) were doped into the $0.76(0.94Bi_{0.5}Na_{0.5}TiO_3\text{-}0.06BaTiO_3)\text{-}0.24Sr_{0.7}Bi_{0.2}TiO_3$ (BNBT-SBT) ceramics to enhance the E_b and further disrupt the long-range order, which is the main research content. Finally, a superior W_{rec} of 4.4 J cm^{-3} and an ultrahigh η of ~91% are achieved in the La doped BNBT-SBT ceramic simultaneously. At the same time, the energy storage performance keeps stable in the temperature range of 30–120 °C, the wide frequency range of 1–100 Hz, and even after 10^6 electrical cycles. These results prove that the La-doped BNBT-SBT ceramic could be a promising candidate for lead-free energy storage capacitors.

The details of samples preparation and characterization are described in the supplementary material. The XRD patterns of Re_2O_3 (Re = La, Er, and Nd) doped BNBT-SBT ceramics corresponding to different rare-earth elements at room temperature are shown in Fig. 1(a). Apparently, all samples exhibit a single perovskite structure with no obvious heterogeneous phases, which indicates that rare-earth elements could diffuse into the lattice of the BNT-based matrix to form solid solutions. To further reveal the phase structure of all samples, the (200) peak is enlarged and displayed in Fig. 1(b). It can be seen that the diffraction peak at about 46°–47° owns a very near splitting peak of all the samples, which are obvious but not strong in intensity. This phenomenon implies a coexistence of a tetragonal phase (P4 mm) and a pseudocubic phase (Pm3m).[20] The pseudocubic phase usually owns a centrosymmetric-like structure with weak polar, having a significant contribution to the relaxor behavior.[7] In addition, the diffraction peak of the rare-earth doped ceramics is obviously shifted to the higher diffraction angles, which indicates that the lattice constant of the ceramics is shrinking and the cell is contracting.[21] This is mainly due to the fact that A-site Bi^{3+}(1.38 Å) and Na^{+}(1.39 Å) are partially replaced by rare-earth elements with smaller ionic radii [La^{3+}(1.36 Å), Nd^{3+}(1.27 Å)], in which the coordinate number is 12, and Er^{3+} (0.89 Å) will partially go to the B site with a coordinate number of 6. Considering that the ionic radii of La^{3+} and Nd^{3+} are similar to that of Bi^{3+} and Na^{+} and much lower than that of Ba^{2+} and Sr^{2+}, these two elements preferentially replace Bi^{3+} and Na^{+} sites.[15] To better understand the evolution of the phase structure, the bright-field TEM image and selected-area electron diffraction (SAED) were observed in undoped and La-doped BNBT-SBT ceramics, as shown in Fig. S2. The evident lattice fringes of two ceramic samples are presented in Figs. S2(b) and S2(e). Figures S2(c) and S2(f) display the SAED patterns along $[1\ -1\ 2]_C$ and $[0\ 1\ -1]_C$ directions, respectively, which exhibit good crystalline quality with a pure perovskite structure. This result is in agreement with the results of XRD.[22]

Figure S3 shows the microstructure morphologies and corresponding distribution of average grain sizes for the Re_2O_3 doped BNBT-SBT sintered ceramics. All samples display dense microstructures with fine grain sizes, well-defined grain boundaries, and no obvious porosity, indicating that all the ceramics were sintered well at 1150–1200 °C. It can be clearly seen that the average grain size of all samples is less than 2 μm. Moreover, the doping of rare-earth ions could significantly reduce the average grain size of ceramics, which is consistent with some previous works.[19,23–25] Among the three rare-earth ions, La^{3+} plays the most significant role in reducing the grain size and, finally, results in a decrease in the average grain size from 1.84 to 1.05 μm. This result proves that La^{3+} could act as a valuable grain growth inhibitor for BNT-based ceramics, which is due to the low ion mobility of La^{3+} during the sintering process.[26,27] According to the widely accepted relationship between the E_b and grain size: $E_b \propto 1/\sqrt{G}$,[28] the La^{3+} doped BNBT-SBT ceramic is expected to possess higher E_b, which will be discussed later in detail.

The temperature dependence of dielectric constant (ε_r) and loss ($\tan\delta$) (25–400 °C) measured from 1 kHz to 1 MHz of all samples are presented in Figs. 1(c)–1(f), namely, the dielectric temperature spectrum. Obviously, the temperature spectrum of all samples owns two dielectric anomalies, called T_m and T_s ("s" presents "shoulder" and "m" means "maximum"). The T_s is increased from the relaxor thermal relaxation of PNRs with the rhombohedral and tetragonal matrixs,[8] and T_m originates from the thermal evolution of tetragonal PNRs and rhombohedral to tetragonal phase transition.[9,29] The evident relaxor features could be found in the dielectric temperature spectra of all four systems, including a shift of T_m toward higher temperature with increasing frequency and a typically enhanced dispersive phase

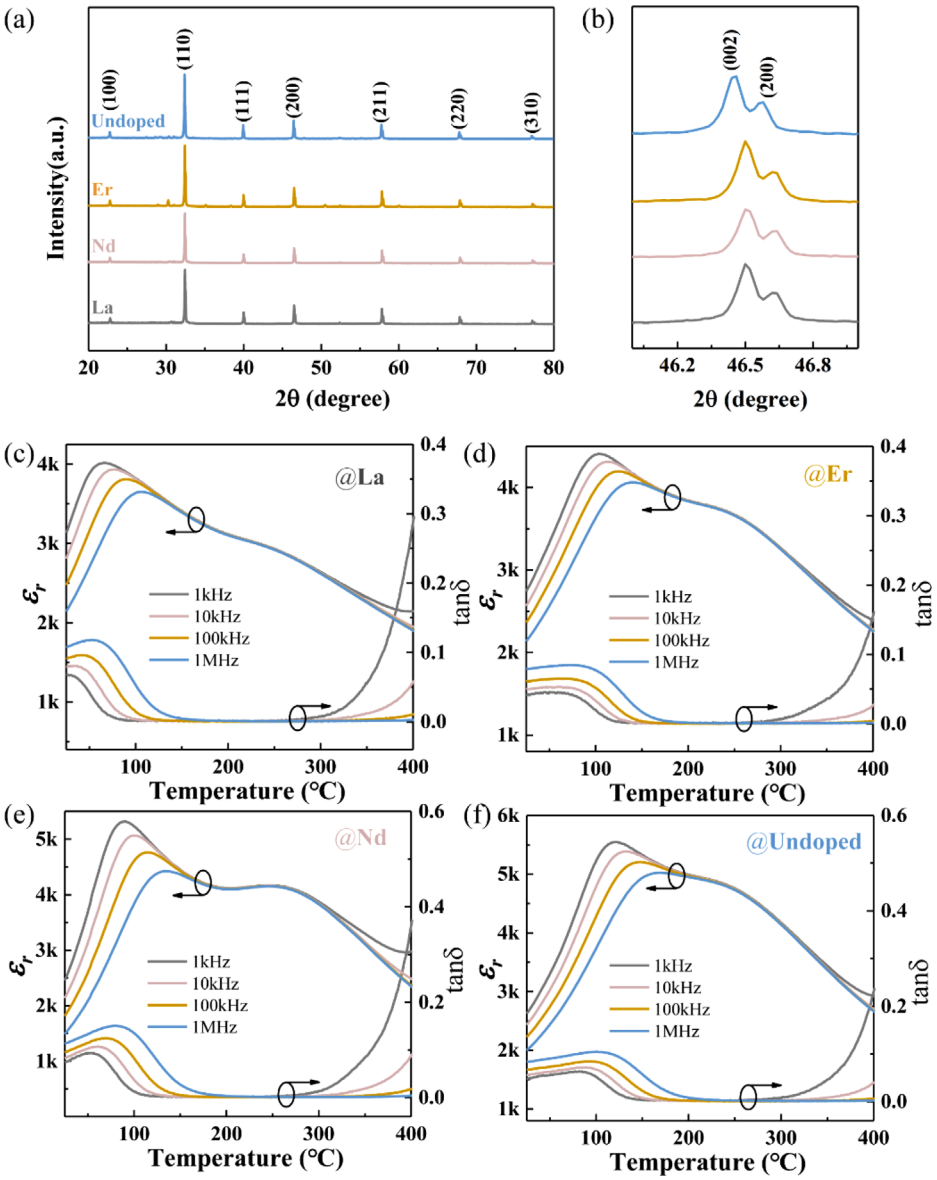

FIG. 1. The (a) XRD profile and (b) enlarged graphs of the (200) peak of rare-earth doped BNBT-SBT ceramics. The temperature dependent dielectric properties measured from 1 kHz to 1 MHz: (c) La, (d) Er, (e) Nd doped, and (f) undoped BNBT-SBT ceramics.

transition behavior. (The peak of T_m becomes depressed and diffused.) These results strongly prove that the doping of rare-earth elements can effectively break the ferroelectric long range order of the original BNT-based ceramics. It is worth noting that tanδ of all ceramics is below 0.3 in all temperature ranges, which helps us to prevent heat loss and ensure the overall value of E_b. tanδ increases again when the temperature exceeds 300 °C, which is probably due to the fact that high temperature activates oxygen vacancies or pores.[30] In addition, both T_m and T_s move toward the lower temperature with the doping of La^{3+} ions. This is due to the fact that the substitution of La^{3+} could enhance the random local field and lead to a gradual increase in the kinetics of PNRs, resulting in a reduced size of PNRs.[21] This phenomenon also confirms to some extent that the La-doped BNBT-SBT ceramic possesses a strong relaxor behavior.

In order to further characterize the dielectric relaxor behavior of all ceramics, the modified Curie–Weiss law: $\frac{1}{\varepsilon_r} - \frac{1}{\varepsilon_m} = \frac{(T-T_m)^\gamma}{C}$ was used for quantitative analysis, where T_m is the temperature at the maximum value of dielectric constant (ε_m) and C is a Curie constant.[31] The relaxor diffuseness factor γ could be obtained directly from the dielectric temperature spectrum using the above formula. Generally, the stronger the relaxor diffuseness, the larger the γ.[32] The relationship between $\ln\left(\frac{1}{\varepsilon_r} - \frac{1}{\varepsilon_m}\right)$ and $\ln(T - T_m)$ is summarized in Fig. S4, and the corresponding factor γ is given in the lower right corner. It can be seen that the relaxor diffuseness factors of rare-earth doped ceramics are improved compared with the undoped BNT-based ceramic. The largest improvement of γ is observed in the La-doped BNBT-SBT ceramic, which is changed from 1.38 to 1.71. The strong relaxor

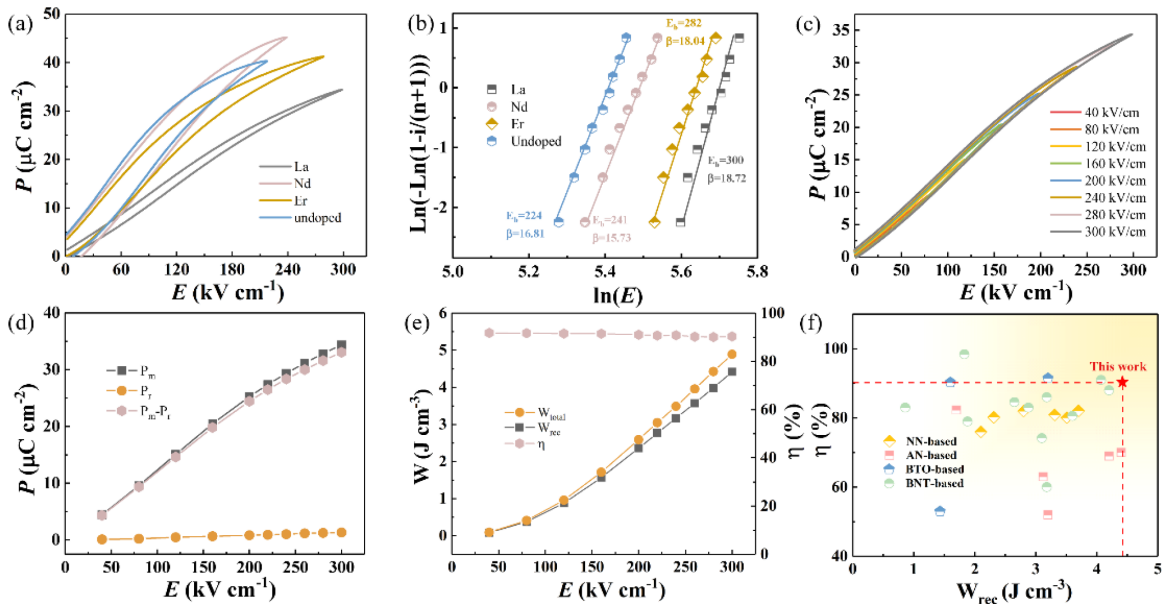

FIG. 2. (a) *P*–*E* loops and (b) Weibull distribution measured under a maximum electric field of all samples. (c)The *P*–*E* loops, (d) P_m, P_r and P_m-P_r and (e) W_{rec}, W_{total} and η under various electric fields of the La-doped BNBT-SBT ceramic. (f) A comparison of W_{rec} and η between the ceramic in this work and other related ferroelectric energy storage systems.

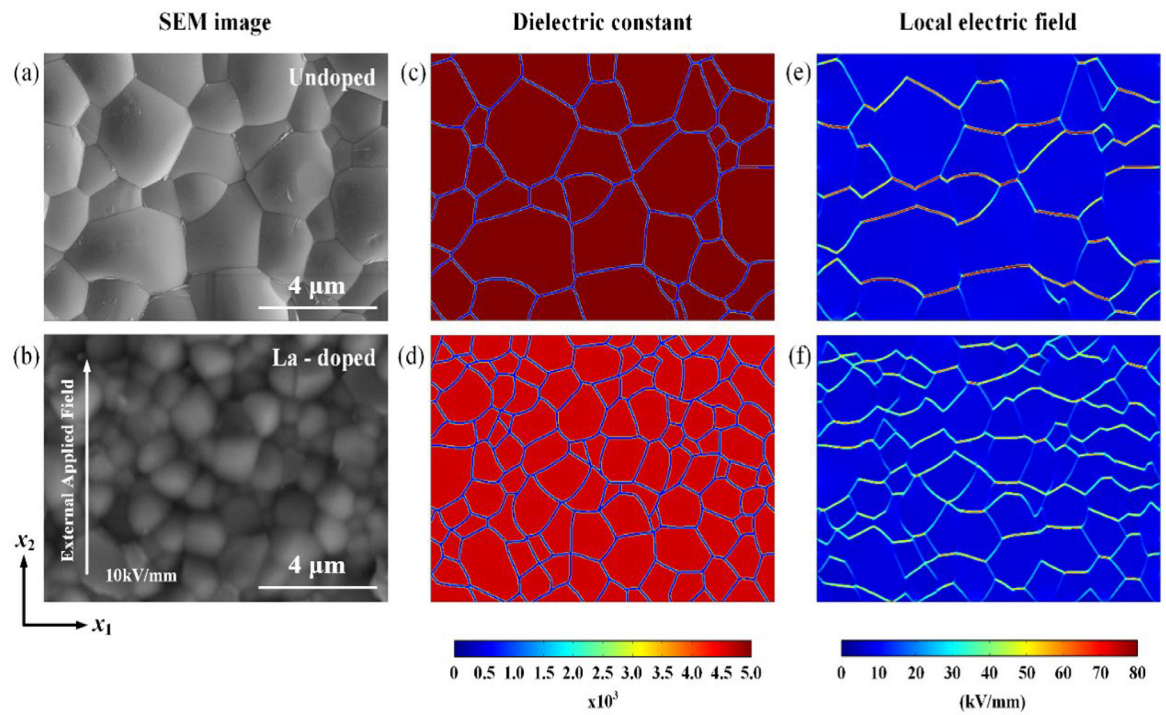

FIG. 3. (a) and (b) Surface morphology, (c) and (d) dielectric constant distribution, and (e) and (f) local electric field distribution of the undoped and La-doped BNBT-SBT ceramics.

behavior of the La-doped BNT-based ceramic is mainly related to the improvement of the random electric/elastic fields induced by the disorder of the local composition.[19] Under the action of rare-earth elements, the random field and local stresses could further weaken the long-range ordered ferroelectric domains and produce more PNRs with weak coupling.[16,27,33] Figure 2(a) shows the unipolar P–E hysteresis loops for all samples at the maximum electric field, and the La-doped BNBT-SBT ceramic possesses a more slender hysteresis loop, indicating an enhanced relaxor behavior in this system. Furthermore, the PFM characterization was employed for microscale observations of domains structures to explain the change of P–E loops (Fig. S5), and the detail is presented in the supplementary material. The above results prove that the long-range ferroelectric order is further disrupted into PNRs by La-doping, and the La-doped BNBT-SBT ceramics possess strong relaxor properties, which could allow the ceramic to own a larger value of P_m-P_r, η, and further high W_{rec}.

In addition to polarization switching behavior, E_b is another important parameter to determine the energy storage performance of ceramics, which could be evaluated via the Weibull distribution. Figure 2(b) displays the Weibull distribution of all ceramic samples, which is fitted by a linear relationship with slope β over 15. This implies that the ceramics own high quality and dependability. The fitting average E_b of Re_2O_3 doped (La, Er, and Nd) and undoped BNBT-SBT ceramics are 300, 282, 241, and 224 kV/cm, respectively, as shown in Fig. S6 with the change in the grain size. Apparently, there is a clear inverse relationship between the E_b and grain size of the ceramics. The E_b value of ceramics is highly related to the nonuniform distribution of local electric fields (LEFs) inside, which is induced by the incorporation of dielectric properties of grain and grain boundaries. The BNBT-SBT ceramics can be seen as composites of high-permittivity grains and low-permittivity grain boundaries, and the volume fraction of the grain boundary is determined by the grain size. The finite element method is used to further explore the influence of the grain size on E_b. The spatial nonuniform distribution of dielectric constants was extracted from the SEM images [Figs. 3(a) and 3(b)] for La-doped and undoped BNBT-SBT ceramics and given in Figs. 3(c) and 3(d). Then the corresponding LEF distributions are simulated by applying an external electric field of 10 kV/mm along the x_2 direction. As plotted in Figs. 3(e) and 3(f), it could be observed that the decrease in grain permittivity and the reduction of grain size, which is induced by the introduction of La-doping, makes the LEF show less inhomogeneity and release from agglomerates around the grain boundaries. According to our previous work,[34] the La-doped sample with more uniform LEF under the same loading of an electric field

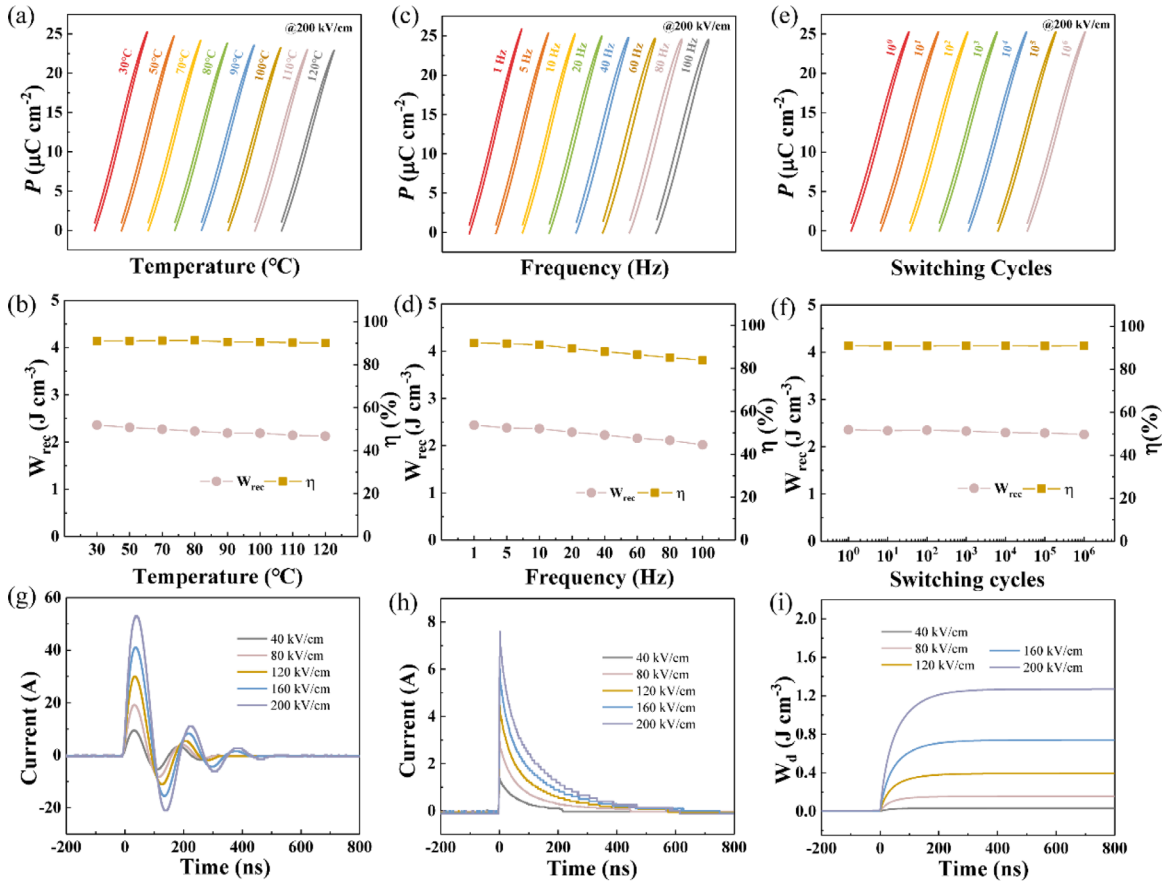

FIG. 4. (a) and (b) Temperature, (c) and (d) frequency, and (e) and (f) fatigue cycles stability; (g) Underdamped charge–discharge curves, (h) overdamped charge–discharge curves, and (i) Wd of the La-doped BNBT-SBT ceramic.

would possess a higher E_b. Hence, the simulation of LEF given here provides a good explanation for the enhanced E_b of the La-doped sample from the aspect of grain size dependence of the LEF distribution.

To characterize the energy storage performance of the La-doped BNBT-SBT ceramic, its unipolar *P–E* loops of under different electric fields are given in Fig. 2(c). The *P–E* loops of the ceramic are very slim over the whole range of the electric field, which also exhibit extremely low P_r. Figures 2(d) and 2(e) summarize the P_m, P_r, P_m-P_r, W_{rec}, W_{total}, and η of the La-doped ceramic. As the electric field rises from 40 to 300 kV/cm, P_m gradually increases to 34.37 μC cm^{-2}, while P_r remains below 1.4 μC cm^{-2}. Finally, an outstanding energy storage density of ~4.4 J cm^{-3} and an ultrahigh efficiency of ~90.36% are obtained under a moderate E_b of 300 kV/cm. Comparisons of W_{rec} and η among AgNbO3-based,[33,35–38] BTO-based,[15,39,40] BNT-based,[4,5,8,41–47] and NN-based[48–53] ceramics are shown in Fig. 2(f), which is used to evaluate the energy storage properties of the La-doped BNBT-SBT ceramic. It is clear that the value of η is below 90% for most lead-free ceramics. Although some BTO-based ceramics own an efficiency of 90%, their W_{rec} is below 4 J cm^{-3}. The moderate energy density and outstanding energy storage efficiency of the La-doped BNBT-SBT ceramic are impressive, suggesting its potential promise for energy storage applications.

The stability of ceramic capacitors subjecting to different environments will further determine the reliability and accuracy of energy storage devices. Figure 4 shows the temperature, frequency, and electric fatigue stability tests of the La-doped BNBT-SBT ceramic under an electric field strength of 200 kV/cm. The temperature-dependent (30–120 °C) *P–E* loops, W_{rec}, and η are shown in Figs. 4(a) and 4(b). The P_m of the ceramic decreases slightly at high temperatures, but its *P–E* loops still remain slim. At the same time, the variation of W_{rec} and η is below 10%, which demonstrates the excellent temperature stability of the ceramics. The La-doped BNBT-SBT sample also displays good frequency stability ($W_{rec} \sim 2.29 \pm 0.24$ J cm^{-3}, $\eta \sim 87.3 \pm 4.1\%$) from 1 to 200 Hz, which is shown in Figs. 4(c) and 4(d). The anti-fatigue properties of energy storage are presented in Figs. 4(e) and 4(f). After the cycling numbers up to 10^8, the variation of W_{rec} and η is below 2%.

Finally, the fast charge–discharge test of the La-doped BNBT-SBT ceramic was conducted to exam its practicability. Figure 4(g) shows the underdamped charge–discharge curves under different electric fields. The current and power density (C_D and P_D) are computed via the equations of $C_D = \frac{I_m}{S}$, $P_D = \frac{EI_m}{2S}$, where I_m, E, and S are the maximum current, electric field, and electrode, respectively. The C_D and P_D display an approximately linear trend with the increase in E, as shown in Fig. S7. Accordingly, the values of C_D and P_D are computed to be 1081.6 A cm^{-2} and 108 MW cm^{-3} under the electric field of 200 kV/cm, respectively. Figures 4(h) and 4(i) display the current–time curves of over-damped discharge performance and corresponding discharge energy density W_d of the selected sample. The W_d is calculated through the formula: $W_d = \frac{R\int I_{(t)}^2 dt}{V}$, where V is the sample volume. The ceramic exhibits an excellent value of W_d (1.27 J cm^{-3}), which is smaller than the result computed from the *P–E* loops. This difference is due to the various test methods and the loss in the dielectric materials caused by the entire resistance-capacitance circuit.[28]

In conclusion, the lead-free Re_2O_3 doped BNBT-SBT ceramics were prepared via the solid-state reaction. The introduction of SBT and rare-earth elements could destroy the long-term ferroelectric order, enhance the PNRs, and then increase the relaxor behavior of the system. Moreover, the rare-earth elements especially La doping reduce the grain size significantly and strengthen the E_b. As a result, the La-doped BNBT-SBT ceramic exhibits an outstanding W_{rec} of ~4.4 J cm^{-3} and an ultrahigh η of ~91% under a moderate electric field of 300 kV/cm. Good temperature (30–120 °C), frequency (1–100 Hz), and electric fatigue (1–10^6 cycles) stability are obtained at the same time. The above results imply that the rare-earth doped BNT-based ceramics own great competitiveness in the energy storage application.

See the supplementary material for the materials and methods, the schematic diagram of a two-steps synergistic design strategy, SEM, grain size distributions, TEM images and SAED patterns, PFM images, plotting of average E_b and grain size of different rare-earth ions' doped BNBT-SBT ceramics, and charge–discharge factors of the La-doped BNBT-SBT ceramic under various electric fields.

This work was financially supported by the National Natural Science Foundation of China (Grant Nos. 12272338, 11972320, and 12192214), the National Program on Key Basic Research Project (Grant No. 2022YFB3807601), the Hunan Provincial Natural Science Foundation of China (No. 2021JJ10006), and the Key Research Project of Zhejiang Laboratory (No. 2021PE0AC02). X. Hou also would like to acknowledge support from the RGC Postdoctoral Fellowship Scheme (No. PDFS2223-5S08) and the PolyU Distinguished Postdoctoral Fellowship Scheme (No. 1-YWBC).

AUTHOR DECLARATIONS

Conflict of Interest

The authors have no conflicts to disclose.

Author Contributions

C.B. and X.H. contributed equally to this work.

Chengwen Bin: Investigation (equal); Methodology (equal); Writing – original draft (equal). **Xu Hou:** Methodology (equal); Writing – original draft (equal). **Luocheng Liao:** Investigation (supporting). **Yuwen Liu:** Methodology (supporting); Writing – original draft (supporting). **Han Yang:** Methodology (supporting); Writing – original draft (supporting). **Yunya Liu:** Writing – original draft (equal). **Jie Wang:** Funding acquisition (equal); Methodology (equal); Writing – review & editing (equal).

DATA AVAILABILITY

The data that support the findings of this study are available within the article and its supplementary material.

REFERENCES

[1]H. Qi, A. Xie, and R. Zuo, Energy Storage Mater. **45**, 541 (2022).
[2]Z. Sun, Z. Wang, Y. Tian, G. Wang, W. Wang, M. Yang, X. Wang, F. Zhang, and Y. Pu, Adv. Electron. Mater. **6**(1), 1900698 (2020).
[3]C. Bin, X. Hou, Y. Xie, J. Zhang, H. Yang, L. Xu, H. Wei, and J. Wang, Small **18**(4), 2106209 (2022).
[4]C. Wu, X. Qiu, L. Chen, C. Liu, H. Zhao, W. Ge, Z. Liu, and M. Yao, J. Alloys Compd. **910**, 164851 (2022).

[5]C. Wu, X. Qiu, W. Ge, C. Liu, H. Zhao, L. Chen, Z. Liu, L. Li, and J. G. Fisher, Ceram. Int. **48**(21), 31931 (2022).
[6]L. Yang, X. Kong, F. Li, H. Hao, Z. Cheng, H. Liu, J.-F. Li, and S. Zhang, Prog. Mater. Sci. **102**, 72 (2019).
[7]W. Ma, Y. Zhu, M. A. Marwat, P. Fan, B. Xie, D. Salamon, Z.-G. Ye, and H. Zhang, J. Mater. Chem. C **7**(2), 281 (2019).
[8]L. Zhang, Y. Pu, M. Chen, T. Wei, and X. Peng, Chem. Eng. J. **383**, 123154 (2020).
[9]D. Hu, Z. Pan, Z. He, F. Yang, X. Zhang, P. Li, and J. Liu, Ceram. Int. **46**(10), 15364 (2020).
[10]C. Yang, J. Qian, Y. Han, P. Lv, S. Huang, X. Cheng, and Z. Cheng, J. Mater. Chem. A **7**(39), 22366 (2019).
[11]C. Yang, P. Lv, J. Qian, Y. Han, J. Ouyang, X. Lin, S. Huang, and Z. Cheng, Adv. Energy Mater. **9**(18), 1803949 (2019).
[12]W. Cao, P. Chen, R. Lin, F. Li, B. Ge, D. Song, Z. Cheng, and C. Wang, Compos. B. Eng. **255**, 110630 (2023).
[13]X. Liu, S. Xue, F. Wang, J. Zhai, and B. Shen, Acta Mater. **164**, 12 (2019).
[14]J. Li, F. Li, Z. Xu, and S. Zhang, Adv. Mater. **30**(32), 1802155 (2018).
[15]Q. Huang, F. Si, and B. Tang, Ceram. Int. **48**(12), 17359 (2022).
[16]P. Zhao, B. Tang, Z. Fang, F. Si, C. Yang, and S. Zhang, Chem. Eng. J. **403**, 126290 (2021).
[17]P. Fu, Z. Xu, H. Zhang, R. Chu, W. Li, and M. Zhao, Mater. Des. **40**, 373 (2012).
[18]L. Li, D. Guo, W. Xia, Q. Liao, Y. Han, Y. Peng, and N. Alford, J. Am. Ceram. Soc. **95**(7), 2107 (2012).
[19]B. Chu, J. Hao, P. Li, Y. Li, W. Li, L. Zheng, and H. Zeng, ACS Appl. Mater. Interfaces **14**(17), 19683 (2022).
[20]J. Guo, X. Fan, J. Zhang, S.-T. Zhang, and B. Yang, J. Eur. Ceram. Soc. **43**(4), 1523 (2023).
[21]H. Ye, F. Yang, Z. Pan, D. Hu, X. Lv, H. Chen, F. Wang, J. Wang, P. Li, J. Chen, J. Liu, and J. Zhai, Acta Mater. **203**, 116484 (2021).
[22]W. Cao, R. Lin, P. Chen, F. Li, B. Ge, D. Song, J. Zhang, Z. Cheng, and C. Wang, ACS Appl. Mater. Interfaces **14**(48), 54051 (2022).
[23]P. Fu, Z. Xu, R. Chu, W. Li, G. Zang, and J. Hao, Mater. Sci. Eng. B **167**(3), 161 (2010).
[24]Y. Zhao, Y. Ge, X. Zhang, Y. Zhao, H. Zhou, J. Li, and H. Jin, J. Alloys Compd. **683**, 171 (2016).
[25]R. Duan, J. Wang, S. Jiang, H. Cheng, J. Li, A. Song, B. Hou, D. Chen, and Y. Liu, J. Alloys Compd. **745**, 121 (2018).
[26]X. Liu, H. Guo, and X. Tan, J. Eur. Ceram. Soc. **34**(12), 2997 (2014).
[27]J. Zhang, Y. Lin, L. Wang, Y. Yang, H. Yang, and Q. Yuan, J. Eur. Ceram. Soc. **40**(15), 5458 (2020).
[28]W. Wang, L. Zhang, R. Jing, Q. Hu, D. O. Alikin, V. Y. Shur, X. Wei, G. Liu, Y. Yan, and L. Jin, Chem. Eng. J. **434**, 134678 (2022).
[29]D. Hu, Z. Pan, X. Zhang, H. Ye, Z. He, M. Wang, S. Xing, J. Zhai, Q. Fu, and J. Liu, J. Mater. Chem. C **8**(2), 591 (2020).
[30]J. Shi, X. Chen, X. Li, J. Sun, C. Sun, F. Pang, and H. Zhou, J. Mater. Chem. C **8**(11), 3784 (2020).
[31]F. Yan, X. Zhou, X. He, H. Bai, S. Wu, B. Shen, and J. Zhai, Nano Energy **75**, 105012 (2020).
[32]C. Bin, X. Hou, H. Yang, L. Liao, Y. Xie, H. Wei, Y. Liu, X. Chen, and J. Wang, Chem. Eng. J. **445**, 136728 (2022).
[33]J. Gao, Y. Zhang, L. Zhao, K.-Y. Lee, Q. Liu, A. Studer, M. Hinterstein, S. Zhang, and J.-F. Li, J. Mater. Chem. A **7**(5), 2225 (2019).
[34]J. Huang, X. Hou, S. Gao, Y. Zhou, H. Huang, Y. He, and Q. Zhang, J. Mater. Chem. A **10**(30), 16337 (2022).
[35]H. Wang, X. Jiang, X. Liu, R. Yang, Y. Yang, Q. Zheng, K. W. Kwok, and D. Lin, Dalton Trans. **48**(48), 17864 (2019).
[36]N. Luo, K. Han, L. Liu, B. Peng, X. Wang, C. Hu, H. Zhou, Q. Feng, X. Chen, and Y. Wei, J. Am. Ceram. Soc. **102**(8), 4640 (2019).
[37]P. Ren, D. Ren, L. Sun, F. Yan, S. Yang, and G. Zhao, J. Eur. Ceram. Soc. **40**(13), 4495 (2020).
[38]L. Zhao, Q. Liu, J. Gao, S. Zhang, and J. F. Li, Adv. Mater. **29**(31), 1701824 (2017).
[39]Y. Qiu, Y. Lin, X. Liu, and H. Yang, J. Alloys Compd. **797**, 348 (2019).
[40]X. Lu, L. Zhang, H. Talebinezhad, Y. Tong, and Z. Y. Cheng, Ceram. Int. **44**(14), 16977 (2018).
[41]L. Zhang, Y. Pu, and M. Chen, Ceram. Int. **46**(1), 98 (2020).
[42]Z. Pan, D. Hu, Y. Zhang, J. Liu, B. Shen, and J. Zhai, J. Mater. Chem. C **7**(14), 4072 (2019).
[43]X. Liu, Y. Zhao, J. Shi, H. Du, X. Xu, H. Lu, J. Che, and X. Li, J. Alloys Compd. **799**, 231 (2019).
[44]C. Wang, F. Yan, H. Yang, Y. Lin, and T. Wang, J. Alloys Compd. **749**, 605 (2018).
[45]X. Wang, X. Wu, D. Yang, J. Yin, and J. Wu, Chem. Eng. J. **447**, 137494 (2022).
[46]N. Weng, J. Zhang, J. Wang, T. Pan, J. Wang, and Y. Wang, J. Am. Ceram. Soc. **106**(5), 2963 (2023).
[47]Q. Zhou, Z. Peng, F. Zhang, Q. Chai, D. Wu, P. Liang, L. Wei, X. Chao, and Z. Yang, Ceram. Int. **49**(12), 19701 (2023).
[48]R. Shi, Y. Pu, W. Wang, X. Guo, J. Li, M. Yang, and S. Zhou, J. Alloys Compd. **815**, 152356 (2020).
[49]J. Ye, G. Wang, M. Zhou, N. Liu, X. Chen, S. Li, F. Cao, and X. Dong, J. Mater. Chem. C **7**(19), 5639 (2019).
[50]N. Qu, H. Du, and X. Hao, J. Mater. Chem. C **7**(26), 7993 (2019).
[51]Z. Yang, H. Du, L. Jin, Q. Hu, H. Wang, Y. Li, J. Wang, F. Gao, and S. Qu, J. Mater. Chem. A **7**(48), 27256 (2019).
[52]L.-F. Zhu, Y. Yan, H. Leng, X. Li, L.-Q. Cheng, and S. Priya, J. Mater. Chem. C **9**(25), 7950 (2021).
[53]X. Dong, X. Li, X. Chen, H. Chen, C. Sun, J. Shi, F. Pang, and H. Zhou, Ceram. Int. **47**(3), 3079 (2021).